Empirical approach to measuring interface energies in mixed-phase bismuth ferrite

Stuart R. Burns [1,*,†] Oliver Paull,[1] Ralph Bulanadi,[1,‡] Christie Lau,[1] Daniel Sando [1,§]
J. Marty Gregg,[2] and Nagarajan Valanoor[1]

[1]*School of Materials Science and Engineering, UNSW Sydney, NSW 2052, Australia*
[2]*Centre for Nanostructured Media, School of Mathematics and Physics, Queen's University Belfast,*
University Road, Belfast BT7 1NN, United Kingdom

In complex oxide heteroepitaxy, strain engineering is a powerful tool to obtain phases in thin films that may be otherwise unstable in bulk. A successful example of this approach is mixed-phase bismuth ferrite ($BiFeO_3$) epitaxial thin films. The coexistence of a tetragonal-like (T-like) matrix and rhombohedral-like (R-like) striations provides an enhanced electromechanical response, along with other attractive functional behaviors. In this paper, we compare the energetics associated with two thickness-dependent strain relaxation mechanisms in this system: domain walls arising from monoclinic distortion in the T-like phase, and the interphase boundary between the host T-like matrix and tilted R-like phases. Combining x-ray-diffraction measurements with scanning probe microscopy, we extract quantitative values using an empirical energy balance approach. The domain wall and phase-boundary energies are found to be 113 ± 21 and 426 ± 23 mJ m^{-2}, respectively. These numerical estimates will help us realize designer phase boundaries in multiferroics, which possess colossal responses to external stimuli, attractive for a diverse range of functional applications.

I. INTRODUCTION

Bismuth ferrite ($BiFeO_3$; BFO) is a multiferroic perovskite oxide which forms in the $R3c$ space group, extensively studied for its room-temperature ferroelectric, electromechanical, and antiferromagnetic properties [1,2]. Although BFO was first synthesized in epitaxial thin-film form in 2003 (Ref. [3]), a dramatic surge in interest—particularly regarding the effects of epitaxial strain—occurred in 2009 upon the discovery of a giant axial ratio phase of BFO ("T-like" or "T' BFO," with $c/a = 1.23$), induced by large ($>4\%$) compressive misfit strains [4]. Under intermediary strain states, the material can also be grown with a mixed-phase microstructure, i.e., partially forming bulklike tilted phases (R-like; R') within a matrix comprising the T-like phase of BFO (Ref. [5]). This "mixed-phase BFO" is commonly observed when the film is grown on lanthanum aluminate ($LaAlO_3$; LAO) substrates, to thicknesses above ~25 nm. In mixed-phase BFO, electrical switching transitions between both structural (T' and R') and polar variants ($+T'$ and $-T'$) [6], doping [7], enhanced response from electromechanical switching [8–13], pinning mechanisms [14], optical effects [15,16], ferroelectric tunnel junctions [17], and deterministic control of phases [18,19]

*stuart.burns@ucalgary.ca
†Present address: Department of Chemistry, University of Calgary, 2500 University Drive NW, Calgary, AB, Canada, T2N-1N4.
‡Present address: Department of Quantum Matter Physics, University of Geneva, 24 Quai Ernest-Ansermet, CH-1211, Geneva 4, Switzerland.
§daniel.sando@unsw.edu.au

have been studied extensively. These films routinely display an increase in mixed-phase population upon increasing film thickness, driven by strain relaxation. Interestingly, in some cases where defects are incorporated throughout the film volume, the formation of the mixed phase can be completely inhibited [20–22]. This complex equilibrium provides a wide scope of stimuli which can locally tailor the functionality of the system.

To accurately describe these stimuli and the associated energy landscape, we require a numerical handle of the physical parameters governing the strain relaxation process. Strain relief in mixed-phase BFO is manifested through the formation of new interfaces, either domain walls (DWs) or interphase boundaries (Fig. 1) [23]. However, an explicit value of the energy density of either of these remains unknown. Having a knowledge of these energy values would help guide studies of new phase space in BFO and similar epitaxial thin-film multiferroics.

Here, we analyze the energy landscape associated with mixed-phase BFO as a function of film thickness within the framework of an energy balance approach and a modification of the general Kittel law [25]. Piezoresponse force microscopy (PFM) and atomic force microscopy (AFM) were used to calculate the periodicities of monoclinic domain walls within the T-like matrix (referred to as T'/T' twins) and the boundaries between coexistent structural phases (T'/R' phase boundaries), respectively. To obtain these periodicities, a substantial amount of data was collected and processed to ensure significant statistical weight. X-ray-diffraction (XRD) techniques were used to quantitatively determine the thickness-dependent strain. Following thermodynamic analyses based on elastic potentials, we deduce

034404-1
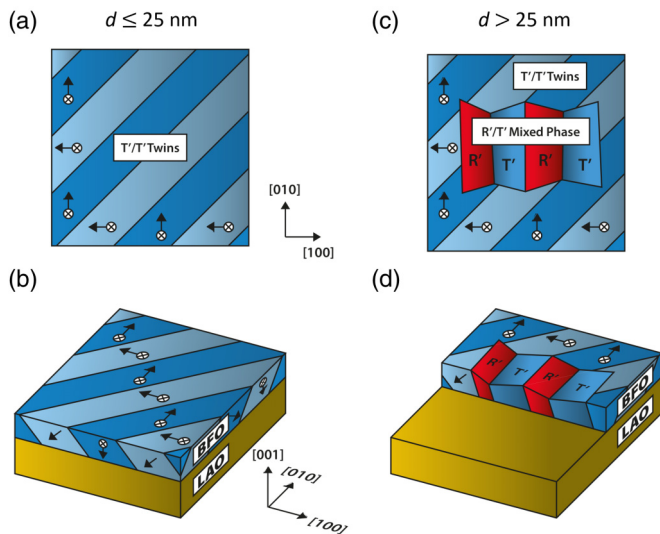
FIG. 1. Schematic of various types of strain-relaxation mechanisms in strongly epitaxially strained BFO films grown on LAO substrates. (a), (b) Only T'/T' twin DWs, which form along $\{1\bar{1}\bar{a}\}$ planes (where a is related to the elastic compliances) [24], are observed for films with thickness below about 25 nm. (c), (d) T'/T' twin DWs as well as T'/R' mixed-phase boundaries are observed for films with thickness above about 25 nm. The arrows denote the local direction of ferroelectric polarization.

values of the energy associated with each of these strain-relief mechanisms.

II. METHODS

A. Thin-film fabrication

BiFeO$_3$ thin films were deposited on LaAlO$_3$ (001) substrates by pulsed laser deposition (PLD), using conditions reported previously [26]. A ceramic target of Bi$_{1.1}$FeO$_3$ was ablated at a repetition rate of 10 Hz using a KrF excimer laser (wavelength of 248 nm) in an oxygen partial pressure of ~0.1 Torr. The laser fluence and film growth rate were measured to be ~1.8 Jcm^{-2} and ~0.04 Å pulse^{-1}, respectively. The substrate was held at a temperature of 590 °C at a distance of ~5 cm from the target. After a predetermined number of pulses dependent on film thickness, each sample was cooled at a rate of 20 °C min^{-1} in an oxygen pressure of 5 Torr.

B. X-ray diffraction and structural characterization

Structural characterization by x-ray diffraction, including high-angle θ-2θ scans and low-angle reflectometry (not shown), was carried out using $K_{\alpha-1}$ radiation ($\lambda = 1.5406$ Å) on a Philips Materials Research Diffractometer, equipped with a two-bounce (220) Ge monochromator. To determine the phase composition (R' and T' phases) and the in- and out-of-plane lattice parameters, reciprocal-space maps (RSMs) were collected on the same diffractometer using a 1D detector (PIXcel). The lattice parameters were calculated by two-dimensional Gaussian peak-fitting the film peaks in the RSMs at each thickness. The uncertainty values for the lattice parameters were calculated from the uncertainty in the position of the peak centers of the 2D Gaussian fits, combined

with the statistical uncertainty when calculating the lattice parameter from the various film spots from the two separate in-plane RSMs (namely 013 and 103).

C. Atomic force microscopy and piezoresponse force microscopy

Topography imaging and ferroic domain mapping were carried out on an Oxford Instruments Asylum Cypher in contact AFM and PFM modes. Due to the fact that T' BFO is monoclinic M_C (Ref. [23]), with an in-plane component of polarization, the PFM data were collected with the lateral displacement channel. Vertical displacement (not shown) provided no contrast in the domain images in the regions of T'/T' walls. The AFM and PFM images were analyzed with WSXM software [27] through both line profiling and image flooding to calculate the periodicities of T'/T' and T'/R' interfaces.

III. RESULTS AND DISCUSSION

We study here a series of BFO films grown on LAO (001). This substrate induces a misfit strain of approximately −4.5%. As previously reported, the film grows in a pure T' phase at the growth temperature (590 °C), but during postgrowth cooling to room temperature, the material relaxes to a mixture of tilted tetragonal-like and rhombohedral-like phases, of which the volume phase fractions are thickness dependent [28–30]. The films had thicknesses of 15–120 nm, as measured by x-ray reflectometry for thinner films (thickness $d < 50$ nm) (not shown), and the growth rate extrapolated to estimate the thicknesses for samples with $d > 50$ nm. This sample set demonstrated the typically observed pure T-like phase in thinner films, while a mixed-phase microstructure was present at higher thicknesses.

To establish a framework which can account for the two aforementioned strain-relieving mechanisms, we must first calculate the strain energies and then periodicities for the T'/T' twins and the mixed-phase interfaces. Thus, we begin with detailed XRD investigations to address the strain energies.

Figures 2(a) and 2(b) present the results of XRD reciprocal-space maps of the 120-nm-thick sample, around the 001 (symmetric) and 103 (asymmetric) reflections (the full maps for all film thicknesses are provided in Figs. S1–S4) [31]. The phases are labeled according to the following convention: T' is the tetragonal-like phase that forms the matrix of the film [the smooth, flat regions in Fig. 1(a)], $T'_{tilt}(R'_{tilt})$ is the tilted T-like (secondary strained R-like) phase which is observed within the mixed-phase regions as striations on the film surface, and $R'_{relaxed}$ is the almost fully relaxed R-like phase (not observed in the AFM images). For the remainder of this paper, for simplicity we use T'/T' to denote the domain walls separating the T-like ferroelastic domains, and T'/R' to denote the interphase boundary between the T'_{tilt} and R'_{tilt} phases.

In the XRD RSMs [Figs. 2(a) and 2(b)] several film-diffraction peaks are observed, which correspond to the various phases related to the striations on the sample surface. We first consider the T' phase. As mentioned above, it is well established that T-like BFO typically forms as an M_C monoclinic structure [29,32]. A signature of such crystallographic symmetry is the threefold splitting of the T-like peak for the
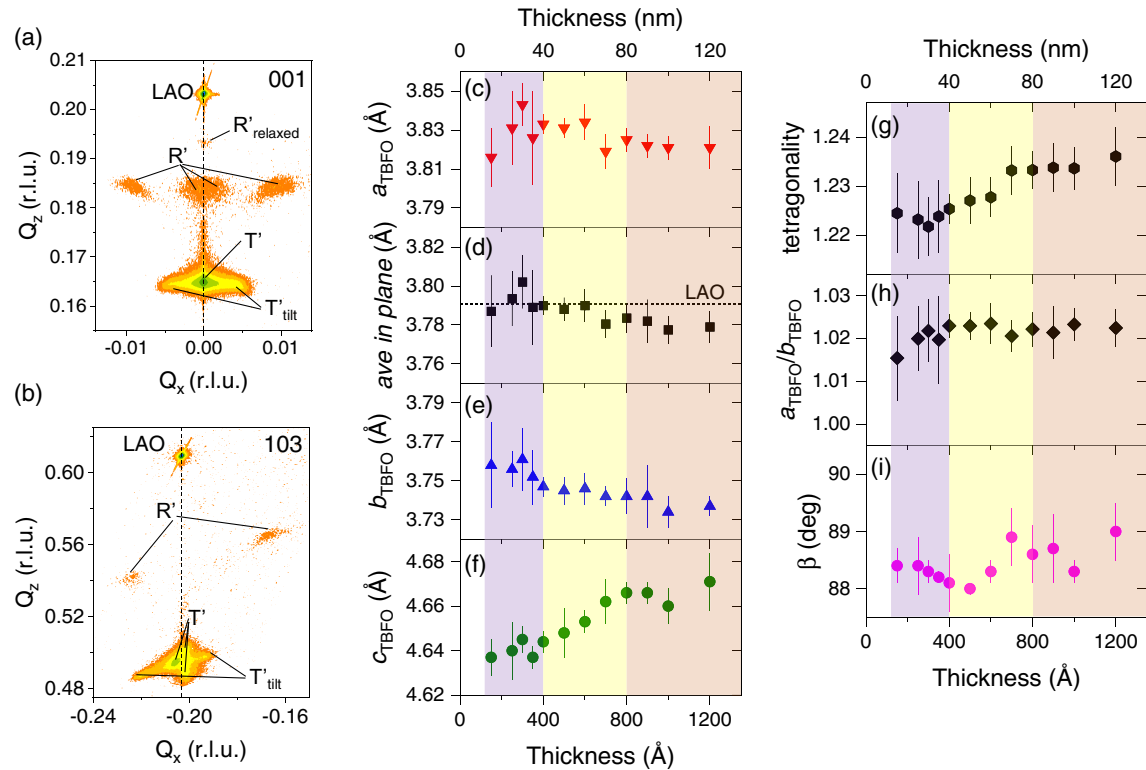
FIG. 2. (a) Symmetric x-ray-diffraction RSM for the 120-nm-thick film near the (001) reflection of LAO and BFO. (b) Asymmetric RSM near the (103) reflection for the 120-nm-thick film, analyzed to calculate in-plane lattice parameters. The threefold splitting of the T' peak is a signature of a monoclinic M_C crystal structure. The dashed- lines in both RSMs indicate the theoretically calculated Q_x value of the corresponding LAO reflection. (c)–(i) a, average in-plane, b, and c lattice parameters, tetragonality, a/b, and monoclinic angle β, of the T-like phase as a function of thickness, respectively. Note the position of the LAO pseudocubic lattice parameter (3.791 Å) with respect to the average in-plane parameters. Three thickness regimes are apparent, as discussed in the main text, and are shaded purple ($\sim$15 to $\sim$40 nm), yellow ($\sim$40 to $\sim$80 nm), and pink ($\sim$80 to $\sim$120 nm).

asymmetric (103) reflection, as labeled in Fig. 2(b). Combining symmetric and asymmetric RSMs measured on the full thickness series of films allows us to calculate the in-plane and out-of-plane lattice parameters of the T-like host matrix. These parameters are shown in Figs. 2(c), 2(e), and 2(f), as well as the average in-plane lattice parameter $\frac{a+b}{2}$ [Fig. 2(d)], the tetragonality $\frac{2c}{a+b}$ [Fig. 2(g)], the distortion a/b [Fig. 2(h)], and the monoclinic angle β [Fig. 2(i)].

Above 10–15 nm, the thickness-dependent behavior of the unit cell in the T-like phase can be separated into three regimes:

(1) $\sim$15 to $\sim$40 nm (shaded in purple): The a and b lattice parameters for films in this thickness range, i.e., prior to nucleation of mixed phase, clearly deviate from the pseudocubic lattice parameter of the LAO substrate (3.791 Å); however, the average in-plane parameter [Fig. 2(d)] is still consistent with that of the substrate. This phenomenon is considered to be a strain relieving mechanism: instead of creating misfit dislocations to relieve strain, the film forms T'/T' domain walls. In this thickness range, the distortion increases with thickness [Fig. 2(h)]. The out-of-plane lattice parameter, c, remains virtually unchanged [Fig. 2(f)].

(2) $\sim$40 to $\sim$80 nm (shaded in yellow): For thickness values at which one would expect the mixed-phase striations to form, the c lattice parameter increases, and the tetragonality of

the unit cell also increases [Fig. 2(g)]. The a and b parameter both decrease gradually.

(3) $\sim$80 to $\sim$120 nm (shaded in pink): When a significant volume of mixed-phase striations is formed in the thickest films, the a and c lattice parameters remain constant while the b parameter continues to decrease slightly. This is seemingly caused by the striations compressing the T-like unit cell. One could suggest that the freedom along the b axis in the T-like phase is linked to the preferential nucleation direction of the secondary phase.

We also used XRD RSMs to determine the lattice parameters of the relaxed R' phases which appear within the mixed-phase striations, by combining the symmetric and asymmetric scans. This was only possible for films of thickness above 70 nm, since for thinner films, the XRD peaks for the secondary R' phase were too weak to obtain reliable parameters. Generally speaking, for the films 70–120 nm thick, the lattice parameters of the R' phase tend only to marginally change for the thickest sample. The in-plane parameter slightly increases, while the out-of-plane parameter falls, with both migrating towards the BFO bulk pseudocubic lattice parameter [33] of 3.965 Å (Fig. S5) [31].

Having characterized the lattice parameters of each film, next we estimated the volume fractions of the R' and T' phases as a function of thickness, particularly at the local scale. This
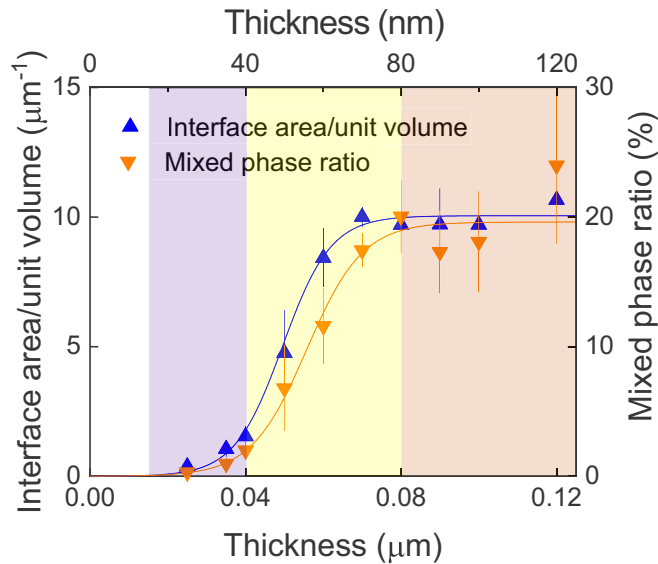
FIG. 3. Average interface density (blue upward triangles) and R'-T' phase ratio (orange downward triangles) as a function of film thickness. The shading is in reference to the thickness regimes discussed in the main text and in Fig. 2. The solid lines are guides to the eye.

thickness dependence of the mixed-phase microstructure is more distinct when imaged through AFM. AFM imaging was carried out across the sample series in order to establish the ratio of mixed phase for a given film thickness (representative data for films 25–120 nm thick are given in Figs. S6–S9) [31]. Alongside this, an image processing technique was applied to quantify the density of the phase interfaces—boundaries between the stripelike structures and their host matrix. Figure S10 presents 5×5-μm^2 topography scans of sample surfaces for three film thicknesses [31], alongside images highlighting the approximate phase interfaces created with the microscopy analysis software described in Ref. [27].

Figure 3 presents the average R' phase percentage and interface density calculated and normalized to the film volume. Note that this is remarkably consistent with the thickness-dependent thermodynamic treatment of Ouyang and Roytburd [34,35]. The weighted-average lattice parameter of the complete microstructure as a function of thickness is plotted

in Fig. S11 [31]. This was calculated by combining the data collected from XRD and AFM and shows the expected behavior of strain relaxation in the system—a decrease of the c parameter and increase in average in-plane lattice parameter above a critical thickness of about 40 nm.

Next, we describe how the periodicities for both the T'/T' domain walls and the mixed-phase interfaces were calculated. In T-like BFO, ferroelastic monoclinic domain structure has been previously reported [36–39]. These periodic walls, arising from the monoclinic distortion of the T-like unit cell, partially minimize elastic self-strain energy [40]. PFM was used to image this domain structure, with the amplitude shown in Figs. 4(a) and 4(b) for 40- and 80-nm-thick films, respectively. In all cases the out-of-plane PFM phase was homogeneous, consistent with the out-of-plane polarization direction pointing downwards (not shown). Here, one can see the presence of tilted-phase striations and ferroelastic DWs in the host T-like phase. All thicknesses studied here exhibited these ferroelastic DWs, implying that they are not as energetically costly as mixed-phase interfaces.

These T'/T' domain walls are aligned along the $\langle 110 \rangle_{pc}$ crystallographic directions (as expected for an M_C symmetry) and terminate at the boundaries between the T-like regions and the mixed-phase striations. The mixed-phase striations themselves are tilted by up to $15°$ from the high-symmetry [100] or [010] directions [Fig. 4(b)] [41,42].

Now that both the strain and periodicity for both types of interfaces have been obtained as a function of thickness, we proceed with the empirical analysis. For this, we start with the key expression employed in this work, Kittel's scaling law for ferroic domain walls [43], given in the general form as

$$ w^2 = \frac{\gamma}{U} d, \tag{1} $$

where w is domain width, γ is the domain-wall energy, U is the domain energy per unit volume, and d is the film thickness. The form of U is dependent on the ferroic order parameter associated with the domain. When empirically adopting this expression, two quantitative results must arise from experiments: (1) an energy term related to the order parameter and (2) a periodicity of the discontinuity manifesting in the ferroic to reduce free energy. In this case, we exclusively consider elastic energy terms.
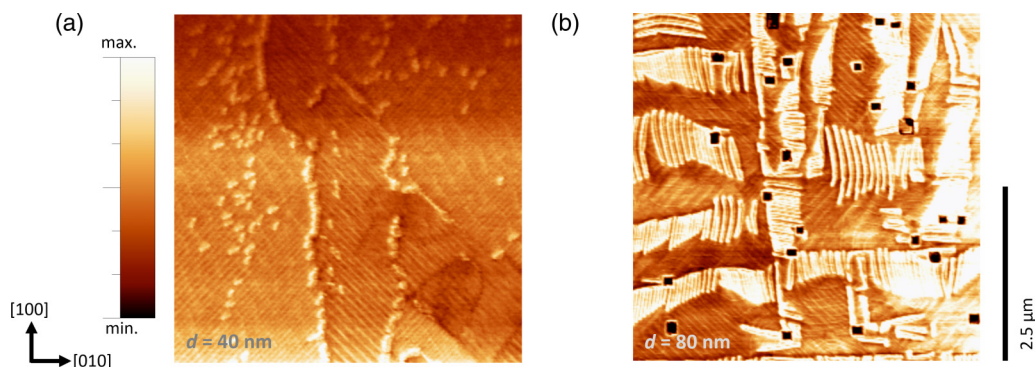

FIG. 4. PFM amplitude images (5×5 μm^2) of (a) 40 nm-thick and (b) 80 nm-thick films, where tilted phase structure and ferroelastic DWs are present.
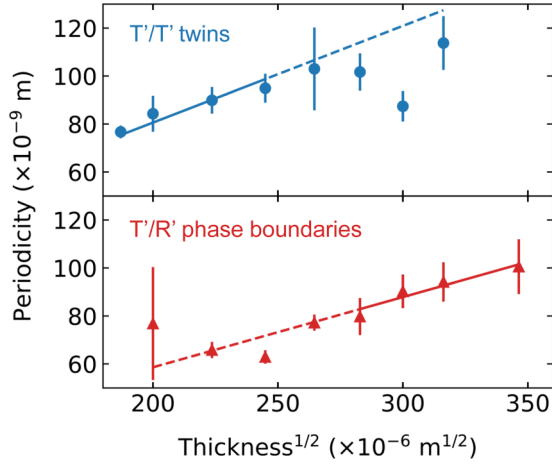
FIG. 5. Periodicity against square root of film thickness of both *T*-like twin domain walls (top) and mixed-phase boundaries (bottom) in the sample series of BFO//LAO (001). The linear fit for each dataset indicates these strain-relieving entities follow Kittel's scaling law ($w \propto d^{1/2}$).

By modifying the general Kittel law expression to add a *second* strain-relieving mechanism, we can incorporate the role of phase interfaces in the analysis alongside the ferroelastic domain walls. As is typical for a Kittel expression, we start from free energy, F:

$$F = A_T \left(U_{T/T} w_{T/T} + \frac{\gamma_{T/T} d}{w_{T/T}} \right)$$
$$+ (1 - A_T) \left(U_{T/R} w_{T/R} + \frac{\gamma_{T/R} d}{w_{T/R}} \right), \quad (2)$$

where A_T and $(1 - A_T)$ are the percentage fractions of *T*-like and mixed-phase regions, respectively, $U_{T/T}$ is the elastic potential energy arising from the *T*-like monoclinic domain walls, and $U_{T/R}$ is the elastic potential energy arising from the formation of mixed-phase regions. The symbols w, γ, and d have their usual meanings (given above), and the subscripts T/T and T/R denote which strain-relieving interface the variables refer to *T*-like domain walls or mixed-phase boundaries, respectively. Taking partial derivatives to describe energetic equilibrium, we arrive at the following relations:

$$\frac{\partial F}{\partial w_{T/T}} = A_T \left(U_{T/T} - \frac{\gamma_{T/T} d}{w_{T/T}^2} \right) = 0; \quad (3)$$

$$\frac{\partial F}{\partial w_{T/R}} = (1 - A_T) \left(U_{T/R} - \frac{\gamma_{T/R} d}{w_{T/R}^2} \right) = 0. \quad (4)$$

All of our samples exhibit T'/T' twins, therefore $A_T \neq 0$. When there is little to no mixed phase in the sample, $(1 - A_T) = 0$, and the equation reduces to the "classic" Kittel law, Eq. (1). From this free-energy expression, one can thus calculate the energy of formation for both the T'/T' twins ($\gamma_{T/T}$) and mixed-phase microstructure ($\gamma_{T/R}$).

Returning to the experiments, we consider next the PFM and AFM-derived periodicities for both T'/T' twins and mixed-phase boundaries. Figure 5 displays the periodicities of both strain-relieving entities as a function of the square root of thickness (with intercept $= 0$), as a linear fitting of

this plot would indicate that the scaling mechanism is following Kittel's law. As there are distinct thickness regions with different behaviors, we isolated the four thinnest films to calculate the periodicity of T'/T' twin walls. Using a similar line of reasoning, the four thickest films were isolated to calculate the periodicity of the phase boundaries. In this way, we identify two separate regimes to which we applied our energy analysis, each following a dense domain-wall model. Rationale for using only these four endpoints in each case is provided later.

We denote the linear fit gradients as $M_{T/T}$ (blue fit, $\approx 4.03 \times 10^{-4}$) and $M_{T/R}$ (red fit, $\approx 2.93 \times 10^{-4}$) for the *T*-like domain walls and mixed-phase boundaries, respectively. The gradients are related to the energy terms through the following equations, where 2π is a shape factor [44] typically used in Kittel expressions:

$$M_{T/T} = 2\pi \left(\frac{\gamma_{T/T}}{U_{T/T}} \right)^{1/2}, \quad (5)$$

$$M_{T/R} = 2\pi \left(\frac{\gamma_{T/R}}{U_{T/R}} \right)^{1/2}. \quad (6)$$

The elastic energy term $U_{T/T}$ was derived from the elastic misfit between the substrate and both the *a* and *b* lattice parameters:

$$\varepsilon_{a_T} = \frac{a_T - a_{\text{sub}}}{a_T}, \quad (7)$$

$$\varepsilon_{b_T} = \frac{b_T - a_{\text{sub}}}{b_T}, \quad (8)$$

$$U_{T/T} = \frac{Y}{1 - \nu} \left(\varphi \varepsilon_{a_T}^2 + [1 - \varphi] \varepsilon_{b_T}^2 \right), \quad (9)$$

where a_T and b_T are the in-plane lattice parameters, a_{sub} is the substrate lattice parameter of 3.791 Å, Y is the Young modulus (186 GPa, taken from Ref. [34]), ν is the Poisson ratio (0.35; Ref. [45]), and φ is the phase fraction of *a*-oriented domains in the region of *T*-like phase, which, if assuming equal T'/T' domain populations, we take $\varphi = 1/2$.

Similarly, the energy $U_{T/R}$ was calculated by consideration of the average in-plane (IP) elastic misfit strains in the region of mixed-phase striations:

$$\varepsilon_{\text{IP}_T} = \frac{\text{IP}_T - a_{\text{sub}}}{\text{IP}_T}, \quad (10)$$

$$\varepsilon_{\text{IP}_R} = \frac{\text{IP}_R - a_{\text{sub}}}{\text{IP}_R}, \quad (11)$$

$$U_{T/R} = \frac{Y}{1 - \nu} \left(\varphi \varepsilon_{\text{IP}_T}^2 + [1 - \varphi] \varepsilon_{\text{IP}_R}^2 \right), \quad (12)$$

where IP_T and IP_R are the average in-plane lattice parameters for the *T*-like and *R*-like striations, and in this case φ is the ratio of *T*-like to *R*-like phases in the areas containing striations, which we assume will reduce to $\varphi = 1/2$, given previous literature [28] identifying the phases of each portion of these needlelike structures.

TABLE I. Reported values of domain-wall energy for $BaTiO_3$, $PbTiO_3$ (first-principles calculations), and $BiFeO_3$ (first-principles calculations and this work).

Material and domain-wall variant	Domain-wall energy (mJ/m^2)	Reference
$BaTiO_3 - 180°$ wall	7.2–16.8	
$PbTiO_3 - 90°$ wall	29.4–35.2	[46]
$PbTiO_3 - 180°$ wall	132–169	
$BiFeO_3 - 71°$ wall	363–436	
$BiFeO_3 - 109°$ wall	205–1811	[47]
$BiFeO_3 - 180°$ wall	829	
$BiFeO_3 - T'/T'$ wall	113 ± 21	
$BiFeO_3 - T'/R'$ phase boundary	426 ± 23	This work

The value of T'/T' domain wall (or phase boundary) energy, $\gamma_{T/T}$ (or $\gamma_{T/R}$) is extracted from the linear fits in Fig. 5:

$$\gamma_{T/T(T/R)} = \frac{U_{T/T(T/R)}M_{T/T(T/R)}^2}{4\pi^2}. \tag{13}$$

From this analysis, the average energy for forming T'/T' twin domain walls is found to be 113 ± 21 mJ m^{-2}, while for forming mixed-phase T'/R' boundaries it is 426 ± 23 mJ m^{-2}. These values, as expected, are consistent with the experimental observation of a critical thickness at which mixed phases form—only at this thickness does the film overcome the cost of forming phase boundaries to relieve strain, whereas the more energetically favorable method of partial strain relief (forming T'/T' twins) occurs at all the thicknesses (above ~15 nm) across our sample range. These values of domain wall and interphase boundary energy are also of the same order of various types of domain walls in $PbTiO_3$ and $BiFeO_3$, as reported in Table I.

IV. DISCUSSION AND CONCLUSIONS

Our empirical approach to determine domain wall and interphase boundaries in the mixed-phase BFO system comes with some caveats, which we briefly discuss here. Recall that our treatment uses two key quantitative results from experiments: (i) a strain-energy term related to the order parameter, and (ii) a periodicity discontinuity, which we ascribe to the system changing the type of interface nucleated in order to reduce the elastic energy. As there is no change of phase in the out-of-plane PFM signal with increasing thickness, we surmise that these domains do not form to minimize depolarization field. Therefore, we have disregarded the electrostatic energies and assume that the formation of T'/T' occurs to minimize the internal self-strain energy arising from the monoclinic distortion of the T-like unit cell. This explains why we exclusively treat the free energy in-elastic energy terms.

Next, we point out that we have not accounted for the curvature of the domain walls. This would require incorporating a gradient term (in the vicinity of the wall) in the strain-energy expression, only possible experimentally by precise mapping of the atomic-level displacements as a function of the distance from the wall. To the best of our knowledge, such information would only be accessible using aberration-corrected transmission electron microscopy which is beyond the scope of this paper. Therefore, we only fitted the first four data points to the

T'/T' twin walls as we are certain with only these four samples the strain state is governed only by the T'/T' twins and not the mixed-phase formation. In the same vein, only the last four data points are fitted to extract the energy for the T'/R' interphase boundaries. It is only in these last four samples that we truly find the dense domain state, which allows us to reasonably disregard the gradient terms [34,48].

Finally, for simplicity, our approach does not take into account the presence of other possible domain arrangements, such as nanotwins which can form parallel to the substrate interface, reported by Pailloux *et al.* [49]. The laser used for PLD grown in that work was Nd:yttrium aluminum garnet (YAG), while for our samples we used an excimer laser. It has been shown that the strongly different growth conditions for the two ablation laser types results in BFO films with different crystallinity, mosaicity, and domain structures [50,51]. Similarly, it is possible that the Nd:YAG laser promotes the formation of such exotic nanotwin defects in BFO//LAO. To the best of our knowledge, excimer grown BFO//LAO samples have not been reported to show such nanotwin structures.

In summary, we have explored the energetics of formation of T'/T' and interphase boundaries in the mixed-phase $BiFeO_3$ thin-film system. Combining XRD, AFM, and PFM techniques, we characterized a series of BFO//LAO (001) films with thicknesses of 15–120 nm. From the XRD data we extracted the lattice parameters for both the T-like and mixed-phase regions, allowing the estimation of elastic strain energies. The periodicities of the T'/T' twin ferroelastic domain walls and mixed-phase T'/R' striations were determined through PFM and AFM analyses, respectively. The energy of formation for domain walls and interphase boundaries were calculated to be $\gamma_{T/T} \approx 113 \pm 21$ mJ m^{-2} and $\gamma_{T/R} \approx 426 \pm 23$ mJ m^{-2}, respectively. These results strengthen our understanding of these strain-relieving microstructures and provide numerical guidelines for the engineering of exotic phases in tailor-made and dimensionally confined [52] multiferroic systems.

[1] G. Catalan and J. F. Scott, Physics and applications of bismuth ferrite, Adv. Mater. **21**, 2463 (2009).

[2] S. R. Burns, O. Paull, J. Juraszek, V. Nagarajan, and D. Sando, The experimentalist's guide to the cycloid, or noncollinear antiferromagnetism in epitaxial BiFeO$_3$, Adv. Mater. **32**, 2003711 (2020).

[3] J. Wang, J. Neaton, H. Zheng, V. Nagarajan, S. Ogale, B. Liu, D. Viehland, V. Vaithyanathan, D. Schlom, U. Waghmare, N. Spaldin, K. Rabe, M. Wuttig, and R. Ramesh, Epitaxial BiFeO$_3$ multiferroic thin film heterostructures, Science **299**, 1719 (2003).

[4] H. Béa, B. Dupé, S. Fusil, R. Mattana, E. Jacquet, B. Warot-Fonrose, F. Wilhelm, A. Rogalev, S. Petit, V. Cros, A. Anane, F. Petroff, K. Bouzehouane, G. Geneste, B. Dkhil, S. Lisenkov, I. Ponomareva, L. Bellaiche, M. Bibes, and A. Barthélémy, Evidence for Room-Temperature Multiferroicity in a Compound with a Giant Axial Ratio, Phys. Rev. Lett. **102**, 217603 (2009).

[5] R. J. Zeches, M. D. Rossell, J. X. Zhang, A. J. Hatt, Q. He, C. H. Yang, A. Kumar, C. H. Wang, A. Melville, C. Adamo, G. Sheng, Y. H. Chu, J. F. Ihlefeld, R. Erni, C. Ederer, V. Gopalan, L. Q. Chen, D. G. Schldin, N. A. Spaldin, L. W. Martin, and R. Ramesh, A strain-driven morphotropic phase boundary in BiFeO$_3$, Science **326**, 977 (2009).

[6] R. K. Vasudevan, Y. Liu, J. Li, W. I. Liang, A. Kumar, S. Jesse, Y. C. Chen, Y. H. Chu, V. Nagarajan, and S. V. Kalinin, Nanoscale control of phase variants in strain-engineered BiFeO$_3$, Nano Lett. **11**, 3346 (2011).

[7] A. R. Damodaran, E. Breckenfeld, A. K. Choquette, and L. W. Martin, Stabilization of mixed-phase structures in highly strained BiFeO$_3$ thin films via chemical-alloying, Appl. Phys. Lett. **100**, 082904 (2012).

[8] Y. J. Li, J. J. Wang, J. C. Ye, X. X. Ke, G. Y. Gou, Y. Wei, F. Xue, J. Wang, C. S. Wang, R. C. Peng, X. L. Deng, Y. Yang, X. B. Ren, L. Q. Chen, C. W. Nan, and J. X. Zhang, Mechanical switching of nanoscale multiferroic phase boundaries, Adv. Funct. Mater. **25**, 3405 (2015).

[9] D. Edwards, N. Browne, K. M. Holsgrove, A. B. Naden, S. O. Sayedaghaee, B. Xu, S. Prosandeev, D. Wang, D. Mazumdar, M. Duchamp, A. Gupta, S. V. Kalinin, M. Arredondo, R. G. P. McQuaid, L. Bellaiche, J. M. Gregg, and A. Kumar, Giant resistive switching in mixed phase BiFeO$_3$ via phase population control, Nanoscale **10**, 17629 (2018).

[10] R. K. Vasudevan, M. B. Okatan, Y. Y. Liu, S. Jesse, J.-C. Yang, W.-I. Liang, Y.-H. Chu, J. Y. Li, S. V. Kalinin, and V. Nagarajan, Unraveling the origins of electromechanical response in mixed-phase bismuth ferrite, Phys. Rev. B **88**, 020402(R) (2013).

[11] D. Mazumdar, V. Shelke, M. Iliev, S. Jesse, A. Kumar, S. V Kalinin, A. P. Baddorf, and A. Gupta, Nanoscale switching characteristics of nearly tetragonal BiFeO$_3$ thin films, Nano Lett. **10**, 2555 (2010).

[12] J. Y. Lee, G. Anoop, S. Unithrattil, W. J. Seol, Y. Yeo, C. H. Yang, S. Y. Lee, and J. Y. Jo, The role of intermediate s-polymorph towards high piezoelectricity in La-doped BiFeO$_3$ epitaxial thin films, Acta Mater. **207**, 116683 (2021).

[13] X. Yin, C. Chen, Z. Fan, M. Qin, M. Zeng, X. Lu, G. Zhou, X. Gao, D. Chen, and J.-M. Liu, Coexistence of multiple morphotropic phase boundaries in strained la-doped BiFeO$_3$ thin films, Mater. Today Phys. **17**, 100345 (2021).

[14] Y.-C. Huang, Y. Liu, Y.-T. Lin, H.-J. Liu, Q. He, J. Li, Y.-C. Chen, and Y.-H. Chu, Giant enhancement of ferroelectric retention in BiFeO$_3$ mixed-phase boundary, Adv. Mater. **26**, 6335 (2014).

[15] D. Sando, Y. Yang, E. Bousquet, C. Carrétéro, V. Garcia, S. Fusil, D. Dolfi, A. Barthélémy, P. Ghosez, L. Bellaiche, and M. Bibes, Large elasto-optic effect and reversible electrochromism in multiferroic BiFeO$_3$, Nat. Commun. **7**, 10718 (2016).

[16] D. Sando, Y. Yang, C. Paillard, B. Dkhil, L. Bellaiche, and V. Nagarajan, Epitaxial ferroelectric oxide thin films for optical applications, Appl. Phys. Rev. **5**, 041108 (2018).

[17] H. Yamada, V. Garcia, S. Fusil, S. Boyn, M. Marinova, A. Gloter, S. Xavier, J. Grollier, E. Jacquet, C. Carrétéro, C. Deranlot, M. Bibes, and A. Barthélémy, Giant electroresistance of super-tetragonal BiFeO$_3$-based ferroelectric tunnel junctions, ACS Nano **6**, 5385 (2013).

[18] J. Zhou, M. Trassin, Q. He, N. Tamura, M. Kunz, C. Cheng, J. Zhang, W.-I. Liang, J. Seidel, C.-L. Hsin, and J. Wu, Directed assembly of nano-scale phase variants in highly strained BiFeO$_3$ thin films, J. Appl. Phys. **112**, 064102 (2012).

[19] Y.-C. Chen, Q. He, F.-N. Chu, Y.-C. Huang, J.-W. Chen, W.-I. Liang, R. K. Vasudevan, V. Nagarajan, E. Arenholz, S. V. Kalinin, and Y.-H. Chu, Electrical control of multiferroic orderings in mixed-phase BiFeO$_3$ films, Adv. Mater. **24**, 3070 (2012).

[20] D. Sando, T. Young, R. Bulanadi, X. Cheng, Y. Zhou, M. Weyland, P. Munroe, and V. Nagarajan, Designer defect stabilization of the super tetragonal phase in >70-nm-thick BiFeO$_3$ films on LaAlO$_3$ substrates, Jpn. J. Appl. Phys. **57**, 0902B2 (2018).

[21] T. Young, P. Sharma, D. H. Kim, T. D. Ha, J. Y. Juang, Y. H. Chu, J. Seidel, V. Nagarajan, S. Yasui, M. Itoh, and D. Sando, Structural, magnetic, and ferroelectric properties of T-like cobalt-doped BiFeO$_3$ thin films, APL Mater. **6**, (2018).

[22] D. Zhang, D. Sando, P. Sharma, X. Cheng, F. Ji, V. Govinden, M. Weyland, V. Nagarajan, and J. Seidel, Superior polarization retention through engineered domain wall pinning, Nat. Commun. **11**, 349 (2020).

[23] D. Sando, B. Xu, L. Bellaiche, and V. Nagarajan, A multiferroic on the brink: Uncovering the nuances of strain-induced transitions in BiFeO$_3$, Appl. Phys. Rev. **3**, 011106 (2016).

[24] J. Erhart, Domain wall orientations in ferroelastics and ferroelectrics, Phase Trans. **77**, 989 (2004).

[25] C. Kittel, Physical theory of ferromagnetic domains, Rev. Mod. Phys. **21**, 541 (1949).

[26] S. R. Burns, D. Sando, B. Xu, B. Dupé, L. Russell, G. Deng, R. Clements, O. H. C. Paull, J. Seidel, L. Bellaiche, N. Valanoor, and C. Ulrich, Expansion of the spin cycloid in multiferroic BiFeO$_3$ thin films, NPJ Quantum Mater. **4**, 18 (2019).

[27] I. Horcas, R. Fernández, J. M. Gómez-Rodríguez, J. Colchero, J. Gómez-Herrero, and A. M. Baro, WSXM: A software for scanning probe microscopy and a tool for nanotechnology, Rev. Sci. Instrum. **78**, 013705 (2007).

[28] A. R. Damodaran, S. Lee, J. Karthik, S. MacLaren, and L. W. Martin, Temperature and thickness evolution and epitaxial breakdown in highly strained BiFeO$_3$ thin films, Phys. Rev. B **85**, 024113 (2012).

[29] W. Siemons, G. J. MacDougall, A. A. Aczel, J. L. Zarestky, M. D. Biegalski, S. Liang, E. Dagotto, S. E. Nagler, and H. M. Christen, Strain dependence of transition temperatures and structural symmetry of BiFeO$_3$ within the tetragonal-like structure, Appl. Phys. Lett. **101**, 212901 (2012).

[30] C. Beekman, W. Siemons, T. Z. Ward, M. Chi, J. Howe, M. D. Biegalski, N. Balke, P. Maksymovych, A. K. Farrar, J. B. Romero, P. Gao, X. Q. Pan, D. A. Tenne, and H. M. Christen, Phase transitions, phase coexistence, and piezoelectric switching behavior in highly strained BiFeO$_3$ films, Adv. Mater. **25**, 5561 (2013).

[31] See Supplemental Material at http://link.aps.org/supplemental/10.1103/PhysRevMaterials.5.034404 for reciprocal-space maps, R'-phase lattice parameters, further AFM images, and the effective lattice parameter as a function of film thickness.

[32] A. R. Damodaran, C. Liang, Q. He, C.-Y. Peng, L. Chang, Y.-H. Chu, and L. W. Martin, Nanoscale structure and mechanism for enhanced electromechanical response of highly strained BiFeO$_3$ thin films, Adv. Mater. **23**, 3170 (2011).

[33] J. M. Moreau, C. Michel, R. Gerson, and W. J. James, Ferroelectric BiFeO$_3$ x-ray and neutron diffraction study, J. Phys. Chem. Solids **32**, 1315 (1971).

[34] J. Ouyang, W. Zhang, X. Huang, and A. L. Roytburd, Thermodynamics of formation of tetragonal and rhombohedral heterophase polydomains in epitaxial ferroelectric thin films, Acta Mater. **59**, 3779 (2011).

[35] W. Zhang, J. Ouyang, and A. L. Roytburd, Effect of thickness-mediated misfit strain on the heterophase polydomain structure of epitaxial BiFeO$_3$ films, Scr. Mater. **66**, 499 (2012).

[36] Z. Luo, Z. Chen, Y. Yang, H.-J. Liu, C. Huang, H. Huang, H. Wang, M.-M. Yang, C. Hu, G. Pan, W. Wen, X. Li, Q. He, T. Sritharan, Y.-H. Chu, L. Chen, and C. Gao, Periodic elastic nanodomains in ultrathin tetragonal-like BiFeO$_3$ films, Phys. Rev. B **88**, 064103 (2013).

[37] C.-S. Woo, J. H. Lee, K. Chu, B.-K. Jang, Y.-B. Kim, T. Y. Koo, P. Yang, Y. Qi, Z. Chen, L. Chen, H. C. Choi, J. H. Shim, and C.-H. Yang, Suppression of mixed-phase areas in highly elongated BiFeO$_3$ thin films on NdAlO$_3$ substrates, Phys. Rev. B **86**, 054417 (2012).

[38] L. You, P. Caesario, L. Fang, P. Ren, L. Wang, Y. Zhou, A. Gruverman, and J. Wang, Effect of lanthanum doping on tetragonal-like BiFeO$_3$ with mixed-phase domain structures, Phys. Rev. B **90**, 134110 (2014).

[39] F. Xue, Y. Li, Y. Gu, J. Zhang, and L.-Q. Chen, Strain phase separation: Formation of ferroelastic domain structures, Phys. Rev. B **94**, 220101(R) (2016).

[40] A. Tagantsev, L. E. Cross, and J. Fousek, *Domains in Ferroic Crystals and Thin Films* (Springer, New York, 2010).

[41] H. Y. Kuo, Y. C. Shu, H. Z. Chen, C. J. Hsueh, C. H. Wang, and Y. H. Chu, Domain pattern and piezoelectric response across polymorphic phase transition in strained bismuth ferrite films, Appl. Phys. Lett. **97**, 242906 (2010).

[42] H. Y. Kuo, Y. C. Shu, H. Z. Chen, C. J. Hsueh, C. H. Wang, and Y. H. Chu, Investigation of nanodomain pattern and piezoelectric behavior of mixed phases in epitaxial BiFeO$_3$ films, J. Eur. Ceram. Soc. **31**, 3063 (2011).

[43] C. Kittel, Theory of the structure of ferromagnetic domains in films and small particles, Phys. Rev. **70**, 965 (1946).

[44] A. Schilling, T. B. Adams, R. M. Bowman, J. M. Gregg, G. Catalan, and J. F. Scott, Scaling of domain periodicity with thickness measured in BaTiO$_3$ single crystal lamellae and comparison with other ferroics, Phys. Rev. B **74**, 024115 (2006).

[45] C. Ederer and N. A. Spaldin, Weak ferromagnetism and magnetoelectric coupling in bismuth ferrite, Phys. Rev. B **71**, 060401(R) (2005).

[46] B. Meyer and D. Vanderbilt, *Ab initio* study of ferroelectric domain walls in PbTiO$_3$, Phys. Rev. B **65**, 104111 (2002).

[47] A. Lubk, S. Gemming, and N. A. Spaldin, First-principles study of ferroelectric domain walls in multiferroic bismuth ferrite, Phys. Rev. B **80**, 104110 (2009).

[48] V. G. Koukhar, N. A. Pertsev, and R. Waser, Thermodynamic theory of epitaxial ferroelectric thin films with dense domain structures, Phys. Rev. B **64**, 214103 (2001).

[49] F. Pailloux, M. Couillard, S. Fusil, F. Bruno, W. Saidi, V. Garcia, C. Carrétéro, E. Jacquet, M. Bibes, A. Barthélémy, G. A. Botton, and J. Pacaud, Atomic structure and microstructures of supertetragonal multiferroic BiFeO$_3$ thin films, Phys. Rev. B **89**, 104106 (2014).

[50] D. Sando, C. Carrétéro, M. N. Grisolia, A. Barthélémy, V. Nagarajan, and M. Bibes, Revisiting the optical band gap in epitaxial BiFeO$_3$ thin films, Adv. Opt. Mater. **6**, 1700836 (2018).

[51] D. Sando, M. Han, V. Govinden, O. Paull, F. Appert, C. Carrétéro, J. Fischer, A. Barthélémy, M. Bibes, V. Garcia, S. Fusil, B. Dkhil, J. Juraszek, Y. Zhu, X. Ma, and V. Nagarajan, Interfacial strain gradients control nanoscale domain morphology in epitaxial BiFeO$_3$ multiferroic films, Adv. Funct. Mater. 2000343 (2020).

[52] S. R. Burns, J. M. Gregg, and V. Nagarajan, Nanostructuring ferroelectrics via focused ion beam methodologies, Adv. Funct. Mater. **26**, 8367 (2016).